EUROPEAN ORGANIZATION FOR NUCLEAR RESEARCH

CERN-PPE/91-01
8 January 1991

Upper Limit for Thermal Direct Photon Production in Heavy-Ion Collisions at 60 and 200 A·GeV

WA80 collaboration

R. Albrecht[1], T. C. Awes[5], P. Beckmann[4,a], F. Berger[4], D. Bock[4], R. Bock[1], G. Claesson[3], G. Clewing[4], L. Dragon[4], A. Eklund[3], R. L. Ferguson[5], A. Franz[b], S. Garpman[3], R. Glasow[4], H. Å. Gustafsson[3], H. H. Gutbrod[1], G. Hölker[4], J. Idh[3], P. Jacobs[2], K. H. Kampert[4], B. W. Kolb[1], P. Kristiansson[3], H. Löhner[4,a], I. Lund[1], F. E. Obenshain[5,b], A. Oskarsson[3], I. Otterlund[3], T. Peitzmann[4], F. Plasil[5], A. M. Poskanzer[2], M. Purschke[4], H. G. Ritter[2], R. Santo[4], S. Saini[5], H. R. Schmidt[1], S. P. Sørensen[5,b], K. Steffens[4], D. Stüken[4], E. Stenlund[3], M. Tincknell[5], and G. R. Young[5]

Abstract

The production of direct photons has been investigated in reactions of p and ^{16}O projectiles at 60 and 200 A·GeV with C and Au nuclei. Photon and π^0 spectra have been measured in the pseudorapidity range $1.5 \leq \eta \leq 2.1$ for the transverse momentum region 0.4 GeV/c $\leq p_T \leq$ 2.8 GeV/c employing the lead-glass spectrometer SAPHIR. An upper limit of 15 % at the 90 % confidence level for the direct photon signal relative to the neutral pion production is obtained from the comparison of measured photon spectra with Monte Carlo simulations of the hadronic background based on the reconstructed yield of π^0 and η mesons. Consequences for a possible phase transition to a quark-gluon plasma are discussed.

(Submitted to Zeitschrift für Physik C)

1. Gesellschaft für Schwerionenforschung (GSI), D-6100 Darmstadt, Fed. Rep. of Germany
2. Lawrence Berkeley Laboratory, Berkeley, California 94720, USA
3. University of Lund, S-22362 Lund, Sweden
4. University of Münster, D-4400 Münster, Fed. Rep. of Germany
5. Oak Ridge National Laboratory, Oak Ridge, Tennessee 37831, USA

a. now at: KVI, University of Groningen, NL-9747 AA Groningen, Netherlands
b. University of Tennessee, Knoxville, Tennessee 37996, USA

1 Introduction

In a first series of experiments with 200 A·GeV ^{16}O ions on heavy targets it has been shown that high energy densities are created up to values where a transition from hadronic matter to a quark-gluon plasma may take place [1]. Out of various signals for detecting this deconfined state, direct photons are considered to be among the most promising since they interact only via the electromagnetic force and therefore leave the reaction zone undisturbed by the hadronic environment. Direct photons have already been measured in p + p and p + A reactions at high transverse momenta ($p_T \geq 3$ GeV/c) [2] where they arise from single hard processes and are calculable by perturbation theory [3, 4]. In the case of a quark-gluon plasma, direct photons are expected as thermal radiation [5, 6, 7] in the region below $p_T \approx 3$ GeV/c, where hard scattering processes have been shown to become small. At very low transverse momenta ($p_T \leq 0.4$ GeV/c) a substantial yield of bremsstrahlung from charged particles may occur [8] which distorts the detection of thermal direct photons. The present experiment was performed in order to explore the possibilities of direct photon detection in the p_T region 0.4 GeV/c $\leq p_T \leq$ 2.4 GeV/c and in the environment of high multiplicities of up to several hundreds of particles per reaction. Since most of the photons arise from π^0 and η decays, a careful investigation of these photon sources and other neutral meson and baryon decays is required. In our experiment, the finely granulated lead-glass detector SAPHIR allows the invariant mass reconstruction of π^0 over the whole p_T range and of η in a restricted one.

2 Experimental

The results presented in this paper were derived from the following detector components of the WA80 setup [9] : the highly segmented lead-glass calorimeter SAPHIR [10], the uranium scintillator sampling calorimeter at zero degree ZDC ($\leq 0.3°$) [11], and the streamer tube multiplicity arrays (SAM, LAM, MIRAM) [12]. SAM and LAM cover the solid angle of SAPHIR. In addition the transverse energy was measured by a lead/iron scintillator sampling calorimeter located at mid-rapidity (MIRAC) [13].

SAPHIR is located at a distance of 342 cm from the target and measures photons from 0.2 to 20 GeV in about 1/6th of the azimuth φ in the pseudorapidity range $1.5 \leq \eta \leq 2.1$. The detector consists of 1278 SF5 lead-glass blocks. The analysis of the photon and neutral pion spectra is restricted to the cuts in azimuthal and polar angles. As the details of the SAPHIR detector have been published elsewhere [10], only the performance characteristics

relevant for this analysis will be described here. In calibration measurements with an electron beam the calorimeter energy resolution was measured to be :

$$\frac{\sigma_E}{E} = 0.4\% + \frac{6\%}{\sqrt{E/\mathrm{GeV}}} \tag{1}$$

A position resolution of 5 mm for an angle of incidence of 15 degrees at 10 GeV/c was obtained by comparing the reconstructed shower position with the incident electron position measured by a delay line wire chamber. Using these resolutions the expected π^0 mass resolution is shown in Fig. 1 for symmetric (solid line) and asymmetric (dashed line) decays. The observed π^0 mass resolution during the operation of the calorimeter at the CERN SPS is also plotted in Fig. 1. Due to the effect of overlapping showers in the high particle multiplicity environment of heavy-ion reactions the observed width is slightly worse than expected from the calibration data. An effective energy resolution of $\sigma_E/E \approx 8.6\%/\sqrt{E/\mathrm{GeV}}$ and a position resolution of 5.9 mm at 10 GeV/c is obtained by a fit to the experimental data.

A maximum nonlinearity in $\Delta E/E$ of 2.3% for photon energies above 0.5 GeV/c has been derived by investigating the variation of the π^0 mass peak position as a function of one photon energy as discussed in detail in Ref. [10, 14].

For the following analysis the streamer tube arrays with pad readout are used as a charged particle veto detector for SAPHIR. Each layer of streamer tubes detects a charged particle with an overall efficiency of 85% and hence an efficiency of $\approx$ 98% is achieved for a logical "or" of the two layers. Assuming the origin of the charged particle in the target the measured position is projected onto the front surface of SAPHIR. Therefore, energy measured in a cluster of SAPHIR modules can be marked by a charged particle veto flag. In Fig. 2 energy spectra of neutral and charged particles from 200 A·GeV ^{16}O+Au reactions are presented. This figure clearly shows a minimum ionizing peak at 540 MeV photon equivalent energy in the charged particle spectrum which is absent in the neutral particle spectrum and confirms the high veto efficiency.

3 Trigger requirements

An event has only been accepted, if the following conditions were fulfilled :

- less than 88% of the total projectile energy is deposited in the ZDC (for ^{16}O beams but not for p beams);
- at least one charged particle is recorded by LAM or MIRAM ($1.2 \leq \eta \leq 4.4$).

With the beam intensity of $\approx 10^6$ ions per spill, an effective spill length of 3.5 seconds, and a target thickness of 186 mg/cm^2 for C (corresponding to a thickness of 0.2% in units of interaction length λ_{int}) and 250 mg/cm^2 for Au (0.1% λ_{int}) it was favourable to apply three additional trigger conditions to enhance the statistics for interesting, e.g. central, reactions. The computer deadtime allowed typically 100 selected events per spill to be written on tape. Two of these triggers enriched the sample of central events relative to more peripheral ones by requiring i) high transverse energy emitted at mid-rapidity and ii) only little energy in the ZDC ($\eta \geq 6.0$). Both quantities are strongly correlated [15] and therefore, these triggers select the same class of events according to their efficiencies and their cut values. The third trigger selected events emitting a photon with a transverse momentum above about 1 GeV/c in the solid angle of SAPHIR. It was found that this trigger works most efficiently in peripheral events, since central events were already selected by the two previously mentioned triggers [16]. The number of analyzed events, reconstructed π^0, and reconstructed γ are given in Tab. 1.

Since the energy measured by the ZDC is dominated by the projectile spectators this quantity characterizes the centrality of each event and is used to distinguish between peripheral and central 200 A·GeV ^{16}O+Au reactions [15]. The cuts applied are $0\,\% \leq E_{ZDC}/E_{BEAM} \leq 30\,\%$ for central and $40\,\% \leq E_{ZDC}/E_{BEAM} \leq 88\,\%$ for peripheral events. In a geometrical picture these cuts correspond to events where all projectile nucleons participate (central) and those events where only a part of the projectile interacts (peripheral).

4 Data analysis

Highly energetic photons (energy $\geq$ 500 MeV) entering the lead glass detector SAPHIR induce electromagnetic showers which deposit their energy into more than one module depending on energy, angle of incidence, and hit position relative to the module boundaries. Such a group of adjacent modules with a signal above threshold will in the following be called a *cluster*. If two maxima can be found within one cluster, two overlapping electromagnetic showers are assumed and they are separated by using the calculated response of electromagnetic showers [17]. Disentangled particles and clusters with one maximum are called *hits*. For minimum-bias 200 A·GeV ^{16}O+Au collisions the probability to find a cluster with one or two maxima is $\approx$ 87% and $\approx$ 10%, respectively. As already mentioned a cluster is assigned to be neutral or charged according to the information from the multiplicity arrays. In the following data analysis all neutral hits are regarded as photons.

The efficiency of the photon identification will be reported in the next section.

Neutral pions are identified by their decay photons ($\pi^0 \rightarrow \gamma\gamma$) and p_T distributions are obtained by performing the following steps :

i Invariant mass spectra are accumulated for different bins of $|\vec{p_T}| = |\vec{p_T}(\gamma_1) + \vec{p_T}(\gamma_2)|$ (see Fig. 3). Only neutral hits with an energy above 500 MeV are accepted.

ii The π^0 peak area is integrated from 107 MeV/c^2 to 167 MeV/c^2 ($\pm 3\,\sigma$) after subtracting the combinatorial background of the mass spectrum. The background is fitted by a polynomial. Performing this integration for different bins of p_T leads to the p_T distributions.

iii This momentum distribution is corrected for the geometrical acceptance calculated by a Monte Carlo simulation and for the photon reconstruction efficiency.

Details of this method can be found in Ref. [10, 14, 18]. In Fig. 3 invariant mass spectra are shown for central 200 A·GeV ^{16}O+Au and minimum-bias 200 GeV p+Au reactions. The determination of the π^0 peak is more difficult in central 200 A·GeV ^{16}O+Au reactions than in minimum-bias 200 GeV p+Au collisions due to the increase of the mean multiplicity of neutral hits with an energy above 500 MeV from 0.5 to 5.1.

In order to check the geometrical acceptance calculation, distributions of the energy asymmetry

$$\alpha = \frac{|E_1 - E_2|}{E_1 + E_2} \tag{2}$$

from experimental data are compared in Fig. 4 with those from the Monte Carlo simulations. Here E_1, E_2 are the energies of the π^0 decay photons. The distributions agree within the statistical errors for the different bins in transverse momentum, i.e. the energy cut and the geometry are well implemented in the Monte Carlo simulation and the merging of decay photons from highly energetic neutral pions does not occur in the p_T region under consideration.

5 Detection efficiencies

The efficiency of photon detection is limited both by the conversion probability in front of SAPHIR as well as by the ability to identify a photon induced shower in the detector. In the environment of high multiplicity heavy-ion reactions the latter of the two points

becomes of particular importance, since the high probabilities of overlapping showers tends to reduce the efficiency of shower recognition.

In the following we will distinguish between the overlap of a neutral hit with another neutral hit and the overlap of a neutral hit with a charged one. The first kind of overlap introduces different detection efficiencies for the photon and π^0 spectra, because a neutral hit produced by at least two neutral particles is always included in the inclusive photon sample but may not be considered for the π^0 sample if the change in energy and/or position gets too large. The second type of overlapping hits decreases the number of neutral hits.

The efficiencies have been determined by two methods. Their combination leads to the total reconstruction efficiencies for photons and π^0's which have been found to depend on the class of selected events, characterized in the following by the mean multiplicity of all hits, μ_{all}, in the detector.

i The probability ε_γ to identify a photon as a neutral hit has been determined by comparing the π^0 peak contents in invariant mass spectra of neutral-charged pairs compared to the peak contents generated by neutral-neutral pairs. Such an analysis automatically selects only those photons which have only a modest change in energy and/or position, i.e. hits which can contribute to the π^0 peak. This method has already been described in detail in Ref. [10, 18]. It shows that there is no significant p_T dependence of ε_γ [14]. Therefore, a mean value of ε_γ averaged over p_T is applied, which appears to be a linear function of μ_{all}. $< \varepsilon_\gamma >_{p_T}$ drops from 90 % at $\mu_{all} = 1.4$ to 68 % at $\mu_{all} = 21.1$. In the limit μ_{all} going to 0, i.e. extrapolating to events with only one particle we obtain 92%. The deviation from 100% is due to photon conversion in the vacuum chamber, streamer tubes, and the target and is in agreement with independent calculations of the conversion probability.

ii The probabilities of overlapping showers have been determined by the technique of superimposing raw data events with low particle multiplicity and by comparing the particle identification from superimposed events with the identification of the low particle multiplicity events. Starting with minimum-bias 200 GeV p+C , 200 GeV p+Au , and peripheral 200 A·GeV ^{16}O+Au reactions the synthetic events are created by superimposing two, three, and four of those events. Except for the superimposed events with the highest multiplicity, $\mu_{all} = 21.1$, again no significant p_T dependence is found for the

overlapping probabilities. It was assumed that neutral hits with an energy change of $|\Delta E/E|$ less than 3% can still contribute to the π^0 peak.

Taking into account the photon conversion probability (derived from ε_γ) three efficiencies have been plotted as a function of the mean multiplicity μ_{all} in Fig. 5. The data points represent the results extracted from the two methods described above. Further reduction of the errors is achieved by using three additional results leading to the final efficiencies given as shaded areas in Fig 5.

A first restriction of the errors arises from the observed frequency of different classes of clusters. It has been found that for the event class with the highest multiplicity only 70% of all detected hits with a transverse momentum above 0.4 GeV/c are photons. The remaining 30% of detected hits, however, cannot be produced by baryons or charged pions since the hadronic energy deposition should be negligible in this p_T region (compare Fig. 7 for neutron energy deposition).

The second constraint stems from a comparison of the π^0 production from the event generator FRITIOF [19] with the measured π^0 production. A number of different experiments [20] have shown that the multiplicity distributions of charged particles at midrapidity are reasonably well described by the event generator . Therefore it can be assumed that the π^0 production is also reasonably well described by FRITIOF. The experimental $\pi^0\, p_T$ spectra have been compared to the FRITIOF distributions with regard to the absolute normalization disregarding the slope of the spectra which is known to deviate from experiment at large values of p_T. The comparison at low and high particle multiplicities agree within the expected uncertainty (see also section 8).

A third important check is deduced by the method of comparing the $\pi^0\, p_T$ distribution of peripheral 200 A·GeV ^{16}O+Au events with the distribution obtained from the four times superimposed events. In Fig. 6 the ratio of the p_T distributions is plotted together with invariant mass spectra calculated from peripheral and superimposed events. The relative efficiency for photons which still contribute to the π^0 signal is calculated from this ratio to be (67 $\pm$ 4) % assuming no p_T dependence.

These results lead to the following efficiencies (see Fig 5):

i efficiency for neutral hits having no or only a small energy and/or position distortion (dotted area, κ_{π^0}). These photons will contribute to the π^0 peak. Therefore, this efficiency is used for correcting the $\pi^0\, p_T$ distributions.

ii efficiency of all neutral hits, in addition to the previous point neutral hits

which will not contribute to the π^0 peak are also taken into account (dashed area, κ_γ). This efficiency is used for correcting the photon p_T spectra.

iii efficiency of all hits which may consist either of an overlap of two or more neutral hits or an overlap of a neutral and a charged one as well as including all true single hits. (solid area)

The difference between the solid and the dashed area represents the probability to assign a neutral hit as a charged particle due to an overlap with a charged particle. The difference between the solid area and the 92% level accounts for the loss of a neutral hit due to overlap of two or more neutral hits. [1]

Neutrons also fulfill the requirements for a neutral hit and are misinterpreted as a photon in this analysis. The ratio of neutrons to photons emitted into the solid angle of SAPHIR has been estimated by the event generator FRITIOF and is about 0.87 in the p_T region above $p_T = 0.4$ GeV/c. Simulations with the code CALOR [21] demonstrate that only a small fraction of the neutron energy is deposited in the one interaction length of the lead-glass modules. This behaviour is illustrated in Fig. 7. The transverse momentum spectra for photons and neutrons emitted into SAPHIR's solid angle are shown as dashed and solid lines, respectively, whereas the visible p_T spectrum for neutrons is displayed as shaded area. In order to describe the detector response, the ADC digitization and the cluster identification algorithm have been applied. Based on this analysis the neutron response can safely be neglected in the following. Analogous results [22] have also been obtained by using the event generator HIJET [23].

6 Background from resonance decays

The direct photon to π^0 ratio (γ/π^0) is extracted from the measured photon yield N_γ and the measured pion yield N_{π^0} according to the expression [2] :

$$\frac{\gamma}{\pi^0} = \frac{N_\gamma}{N_{\pi^0}} \cdot \frac{\kappa_{\pi^0}^2}{\kappa_\gamma} \cdot A_{geo} - (R_{\pi^0} + R_i) \tag{3}$$

where R_{π^0} and R_i are the Monte Carlo calculated ratios of observed background γ's from π^0 decays (R_{π^0}) and from any other sources (R_i) to reconstructed π^0's, and A_{geo} is the geometric acceptance for π^0's.

Besides photons originating from π^0 decays there are several other photon sources which could mimic a direct photon signal. In this section we will discuss the different

[1] These investigations show that the photon reconstruction efficiency for $\pi^0 p_T$ spectra is slightly higher for high multiplicity events than deduced in Ref. [18].

hadronic sources which have to be considered for the photon production and calculate their photon contribution relative to the yield of reconstructed neutral pions. The following points have to be taken into account :

i the production rate and the phase space distribution of the hadrons used in the Monte Carlo simulation,

ii the branching ratio of the hadrons into photons,

iii the available phase space for the decay into photons.

All those hadrons which produce photons through the π^0 channel do not have to be taken into account as these neutral pions are already contained in the measured $\pi^0\, p_T$ distributions. The only exception are hadrons with a long lifetime; these decays will be discussed later. In Tab. 2 the rest mass, decay channel, branching ratio, and the Q-value (= difference between the hadron rest mass and sum of the decay product rest masses) of all hadrons are listed which decay directly into at least one photon with a branching ratio above 1% and whose rest mass is lighter than 1500 MeV/c^2. The production rate of hadrons with a higher rest mass is assumed to be negligible. The decays of the hadrons are generated by the program JETSET 6.3 [25]. In Fig. 8 the transverse momentum of the hadron is plotted versus the transverse momentum of the produced decay photon for the mesons η, η', ω, and the baryon Σ^0. It is obvious that the photon production is controlled by the Q-value, e.g. the Q-value for the decay $\Sigma^0 \rightarrow \Lambda\,\gamma$ is only 76.9 MeV/c^2 and hence a negligible number of photons with $p_T \geq 0.4$ GeV/c will be generated. On the other hand the decays $\eta \rightarrow \gamma\gamma$, $\eta' \rightarrow \gamma\gamma$, and $\omega \rightarrow \pi^0\gamma$ do have a high Q-value and have to be considered. According to the Q-value of 471.2 MeV/c^2 the ϕ meson should also be taken into account, however, due to the small branching ratio of 1.3% for the decay $\phi \rightarrow \eta\gamma$ and the small production rate estimated from the FRITIOF event generator and p + p data (see Tab. 3) the ϕ meson can be neglected.

As SAPHIR measures neutral pions, their p_T distribution [18] is used in the Monte Carlo calculation. For the other hadrons the p_T spectra are derived from the $\pi^0\, p_T$ spectrum assuming scaling with the transverse mass $m_T = \sqrt{p_T^2 + m^2}$ [26] as

$$f(m_T; h) \;=\; C \cdot f(m_T; \pi^0)\,;\; h = \eta, \eta', \omega. \qquad (4)$$

Using Eq. 4 the ratios of produced mesons h to produced π^0's as a function of p_T are displayed in Fig. 9 for central (square) and for peripheral (triangle) 200 A·GeV ^{16}O+Au

reactions. For comparison the following frequently used parameterization [27] has been plotted as dashed lines :

$$f(p_T;h) \;=\; C \cdot f(p_T;\pi^0) \cdot \left(\frac{m_T(\pi^0)+2\,\mathrm{GeV/c^2}}{m_T(h)+2\,\mathrm{GeV/c^2}}\right)^{12.3} \quad ;h \;=\; \eta,\eta',\omega. \tag{5}$$

The normalization points for Eq. 5 are given in Tab. 3 and are taken from p + p data at approximately the same nucleon nucleon center of mass energy. Both parameterizations show a similar p_T dependence and as there are no precise heavy-ion data yet available in order to distinguish between the two curves, Eq. 4 is chosen for our Monte Carlo simulation.

The η production is measured with SAPHIR for minimum-bias 200 A·GeV ^{16}O+Au reactions in the p_T region 2 GeV/c $\leq p_T(\gamma\gamma) \leq$ 2.4 GeV/c (see Fig. 10). The extracted η/π^0 ratio of $(61 \pm 20)\%$ is consistent with the η/π^0 ratio of Fig. 9 and p + p data within the statistical errors.

Fig. 11 displays the Monte Carlo results for the inclusive γ/π^0 ratio. Besides π^0 decays the decay $\eta \rightarrow \gamma\gamma$ is the most important hadronic photon background and introduces the largest uncertainty in this calculation due to the large statistical error of the measured η/π^0 ratio. Photons from ω and η' decays contribute two orders of magnitude less compared to photons from π^0 decays. Hence the uncertainties in the ω and η' production rates contribute to the error, at most 1% of the total γ/π^0 ratio.

Since our detector setup does not allow vertex reconstruction the target is always assumed as the vertex. Therefore, neutral pions decaying several cm from the target cannot be fully reconstructed even if both decay photons are observed. These photons are possible source for false direct photon assignment. As mentioned above weak decays like $K^0_S \rightarrow \pi^0\pi^0$, $\Lambda \rightarrow n\pi^0$, $\Sigma^+ \rightarrow p\pi^0$, and $\Xi \rightarrow \Lambda\pi^0$ can produce such neutral pions. The comparison of the particle rest mass, the branching ratio, and available decay phase space lead to the conclusion that the dominant source for those π^0's are the decays $K^0_S \rightarrow \pi^0\pi^0$. The simulated invariant mass spectrum for π^0's from K^0_S is shown in Fig. 12 a). The different shaded areas indicate the mass region inside and outside the accepted π^0 interval. Due to time dilation the ratio ρ_τ of π^0's inside the accepted mass window to the total number of π^0's is a function of transverse momentum (see Fig. 12 b)) and decreases from 98% at p_T = 0.6 GeV/c to about 75% at p_T = 2 GeV/c. Taking a K^0_S production rate comparable to the production rate of the FRITIOF event generator, which is supported by experimental heavy-ion data [32], the ratio of photons from K^0_S to π^0 as a function of transverse momentum is plotted in Fig. 12 c) giving an upper limit for misidentified direct photons of $\gamma/\pi^0 \leq 10^{-3}$ which can be neglected.

7 Error discussion

In Tab. 4 all systematic and statistical absolute errors entering for the final γ/π^0 evaluation are listed. These sources of uncertainty will be discussed in the following :

- The statistical error of the experimental γ/π^0 data is mainly due to the number of reconstructed π^0's and the π^0 peak to combinatorial background ratio in the invariant mass spectrum.

- The uncertainty of the geometrical π^0 acceptance is caused by an uncertainty of $\pm$ 50 MeV in the energy threshold of 500 MeV due to finite energy resolution and by the assumption that the π^0 transverse momentum distribution is not correlated with the π^0 angular distribution in SAPHIR's solid angle. The second point has been verified [14, 22] by comparing the acceptance calculation with the geometrical acceptance deduced from the event generators HIJET and FRITIOF.

- An upper limit for the nonlinearity $\Delta E/E$ has already been given in section 2. The π^0 and photon p_T spectra are corrected for a mean shift in energy scale observed by the position of the π^0 invariant mass peak leaving an upper uncertainty of $\pm$3%.

- The method of superimposing events introduces systematic errors for the photon reconstruction efficiencies which are caused by the fact that even peripheral 200 A·GeV ^{16}O+Au events have a mean multiplicity of $\mu_{all} = 7$ and therefore already contain a certain number of overlapping showers which cannot be resolved. Therefore, the systematic error increases with increasing mean multiplicity μ_{all}. However the absolute error for the reconstruction efficiencies is reduced by taking into account the three other constraints discussed in section 5.

- The veto efficiency for charged particles is 98%, hence 2% of all charged particles are misidentified as photons. However, similar estimates as for the detector response of the neutrons lead to a conservative upper limit of +0.1% for the direct photon yield in the p_T region above 0.4 GeV/c.

- With the presently existing heavy-ion data it is impossible to evaluate an absolute error of the m_T-scaling. The error is estimated by the difference of the two m_T-scalings from eq. 4 and 5 to be less than 1% in the p_T region under consideration here.

- The error of the hadronic background simulation is mainly due to the uncertainty of the η/π^0 ratio. Other quantities like the detailed rapidity densities of the different mesons in the region of experimental acceptance or the η'/π^0 and ω/π^0 ratios are of minor influence.

The quadratic sum of these errors is $\pm(9-12)\%$ depending on the particle density. Different from Ref. [33] our errors are applied to individual p_T-bins and not to the integrated γ/π^0 ratio. It should also be mentioned that some errors are correlated which would shift all experimental points up or down as a whole.

8 Results

In Fig. 13 a), b) the π^0 and photon p_T distributions for peripheral and central 200 A·GeV ^{16}O+Au reactions (solid circles) are compared separately with the Monte Carlo simulations (histograms). The p_T distributions calculated by the event generator FRITIOF serve as a reference (solid squares). The deviation for increasing p_T values between the data and the model supports the recently discussed rescattering effect of produced particles [34], which is more pronounced in central reactions and not included in the applied FRITIOF version 1.6. The input and output of the Monte Carlo simulations, namely the π^0 and photon p_T spectra, are shown as histograms. The π^0 p_T distributions are normalized to the experimental data and this normalization is kept for the corresponding photon distributions. In order to compare the relative normalization and the p_T dependence between the Monte Carlo results and the experimental data the ratio of both distributions are plotted as an insert in Fig. 13 a), b) showing that the p_T dependence of the measured and predicted photon spectra does not deviate significantly.

A possible excess of direct photons can be more easily observed by comparing the inclusive photon spectrum divided by the inclusive π^0 spectrum from experimental data and from the Monte Carlo calculations. This is shown in Fig. 14 for the systems 200 GeV p+C , 200 GeV p+Au , 200 A·GeV ^{16}O+C , and 60 A·GeV ^{16}O+Au under minimum-bias trigger conditions. In this figure the squares indicate the experimental data and the shaded histograms are Monte Carlo results based on measured π^0 spectra and represent the hadronic background. The difference between data and the histograms can be attributed to the contribution of direct photons. For all four systems the p_T dependence of the data is reproduced by the Monte Carlo simulations. The data for the ^{16}O-induced reactions are approximately 10% above the prediction, but this finding is still within the systematic uncertainty of the data (see also section 7).

The possible transition to a quark-gluon plasma state is expected to occur more likely in central than in peripheral reactions. The 200 A·GeV ^{16}O+Au data (sample with the highest statistics) have thus been divided into peripheral and central events, as already explained in section 3. The data for central 200 A·GeV ^{16}O+Au events (displayed in Fig. 15) show a slight overall enhancement over the hadronic background which is, however, within the statistical and systematic errors. Collecting all sources of uncertainties and assuming them to be gaussians, we arrive at an upper limit of 15% for the contributions of direct photons to the γ/π^0 signal at a confidence level of about 90%.

9 Discussion

The observed similarity in the invariant π cross sections between the peripheral 200 A·GeV ^{16}O+Au and p + p spectra including the onset of hard scattering [18] suggests a similarity in the reaction mechanism and therefore in the direct photon production. In p + p reactions the direct photon yield was found to be vanishingly small at $p_T \approx 2-3$ GeV/c [35, 36]. In addition direct photons have been measured for high transverse momenta in p-induced reactions on light mass targets [37, 38]. These data agree with our results from p-induced events in the limited p_T region of overlap. Our data extend the direct photon analysis to lower p_T-values.

Inclusive photon production has been studied for 0.1 GeV/c $\leq p_T \leq$ 1.5 GeV/c by the HELIOS Collaboration [33] using the conversion method where no π^0's were reconstructed. The hadronic background photons were instead calculated by assuming relations between measured charged pion cross section and the π^0 yield. In the region of mutual overlap (0.4 GeV/c $\leq p_T \leq$ 1.5 GeV/c) the photon data agree and are compatible with a purely hadronic origin.

To summarize, we have demonstrated that with a finely granulated lead-glass detector a direct photon analysis based on π^0 reconstruction is feasible even in the high multiplicity environment of heavy-ion reactions. The data presented here cover a p_T range of 0.4 GeV/c $\leq p_T \leq$ 2.8 GeV/c, which corresponds to the region where thermal direct photons from a possible quark-gluon plasma are expected. The present analysis sets an upper limit of $\gamma_{direct}/\pi^0 \leq 15\%$ on the signal for all systems investigated. Different predictions about the magnitude of the expected effect have been made [7, 39, 40] depending on the assumptions about the formation of the deconfined state and its physical parameters. The achieved accuracy does not yet allow to discriminate between these predictions. However, considering the different sources of errors it is expected that the uncertainty of

the γ_{direct}/π^0 ratio can be reduced to the level of few percent by increasing the detector coverage and the number of events. Such an accuracy will be sufficient to attack the direct photon detection in forthcoming experiments with heavier projectiles.

This work was partially supported by the West German BMFT and DFG, the VW-Stiftung, the United States DOE, the Swedish NFR, and the Alexander von Humboldt Foundation.

References

[1] *Quark Matter*, Z. Phys. **C** - Particles and Fields **38** (1988), H. Satz, H. Specht and R. Stock, eds., and references therein

[2] T. Ferbel and W. R. Molzon, Rev. Mod. Phys. **56** (1984) 181

[3] J. F. Owens, Rev. Mod. Phys. **59** (1987) 465

[4] P. Aurenche, R. Baier, M. Fontannaz, and D. Schift, Nucl. Phys. **B 297** (1988) 661

[5] R. C. Hwa and K. Kajantie, Phys. Rev. **D 32** (1985) 1109

[6] L. McLerran and T. Toimela, Phys. Rev. **D 31** (1985) 545

[7] M. Neubert, Z. Phys. **C** - Particles and Fields **42** (1989) 231

[8] E.V. Shuryak, Phys. Rev. **D 42** (1990) 1764-1776

[9] H.H. Gutbrod et al., GSI preprint GSI-85-32, August 1985 and CERN SPSC/85-39/M406

[10] H. Baumeister et al., Nucl. Instr. Meth. **A 292** (1990) 81-96

[11] G. R. Young et al., Nucl. Instr. Meth. **A 279** (1989) 503 - 517

[12] R. Albrecht et al., Nucl. Instr. Meth. **A 276** (1989) 131 - 139

[13] T. C. Awes et al., Nucl. Instr. Meth. **A 279** (1989) 479 - 502

[14] L. Dragon, Doctoral thesis, University of Münster (1989)

[15] R. Albrecht et al., WA80 Collab., Phys. Lett. **B 199** (1987) 297

[16] M. Purschke, Doctoral thesis, University of Münster (1990)

[17] M. Della Negra, Physica Scripta **23** (1981) 469

[18] R. Albrecht et al., WA80 Collab., Z. Phys. **C** -Particles and Fields **47** (1990) 367-375

[19] B. Andersson, G. Gustafson, and B. Nilsson-Almqvist, Nucl. Phys. **B 281** (1987) 289-309
B. Nilsson-Almqvist and E. Stenlund, Comp. Phys. Com. **43** (1987) 387-397

[20] M.I. Adamovich et al.,EMU-01 Collab., Phys. Lett. **B 201** 397-402
R. Albrecht et al., WA80 Collab., Phys. Lett. **B 202** (1988) 596-602
A. Bamberger et al., NA35 Collab., Phys. Lett. **B 205** (1988) 583-589
T. Åkesson et al., HELIOS Collab., Nucl. Phys. **B 333** (1990) 48-65

[21] J. Brau and T. A. Gabriel, Nucl. Instr. Meth. **A 238** (1985) 489

[22] L. Dragon, Diploma thesis, Münster (1985)

[23] T. Ludlam et al.,RHIC Workshop I, eds. P. Haustein and C. Woody (Brookhaven, April 1985), BNL-51921

[24] Particle Data Group, *Review of Particle Properties*, Phys. Lett. **B 204**

[25] T. Sjöstrand and M. Bengtsson, *The Lund Monte Carlo for Jet Fragmentation and e^+ e^- Physics – JETSET version 6.3 – an Update*, preprint : LU TP 86-22
The Lund Monte Carlo Programs, CERN, long writeup, 3. April 1987

[26] J. Bartke et al., Nucl. Phys. **B 120** (1977) 14
E. V. Shuryak, Phys. Rep. **61** (1980) 71-158
E. V. Shuryak and O. V. Zhirov, Phys. Lett. **B 89** (1980) 253-255
E. V. Shuryak, Yellow Report, CERN/**83-01** (1983)
E. V. Shuryak, *The QCD Vacuum, Hadrons and the superdense Matter*, World Scientific Lecture Notes in Physics - Vol.8, (1988)

[27] M. Bourquin and J. M. Gaillard, Nucl Phys. **B 114** (1976) 334

[28] T. Åkesson et al., Phys. Lett. **B 178** (1986) 447

[29] M. Diakonou et al., Phys. Lett. **B 89** (1980) 432

[30] C. W. Ackerlof et al., Phys. Rev. Lett. **39** (1977) 861

[31] J. A. Appel et al., Phys. Rev. Lett. **35** (1975) 9

[32] A. Bamberger et al., NA35 Collab., Z. Phys. **C 43** (1989) 25-35

[33] T. Åkesson et al., HELIOS Collab., Z. Phys. **C 46** (1990) 361-367

[34] A. Shor and R. Longacre, Phys. Lett. **B 218** (1989) 100
K. Werner and P. Koch, Phys. Lett. **B 242** (1990) 251

[35] T. Åkesson et al., AFS Collab., Phys. Lett. **B 123** (1983) 367

[36] E. Anassontzis et al., Z. Phys. **C 13** (1982) 277-289

[37] R. M. Baltrusaitis et al., Phys. Lett. **B 88** (1979) 372

[38] J. Badier et al., NA3 Collab., Z. Phys. **C 31** (1986) 341-347

[39] F. Halzen and H. C. Liu, Phys. Rev. **D 25** (1982) 1842-1846
J. Cleymans, M. Dechantsreiter, F. Halzen, Z. Phys. **C 17** (1983) 341-352

[40] K. Kajantie and H. I. Miettinen, Z. Phys. **C 9** (1981) 341-345

Tables

system		N_{events} $\div 1000$	*reconstructed* π^0 $\div 1000$	*reconstructed* γ $\div 1000$
200 GeV p+C		476	5	15
200 GeV p+Au		572	11	41
200 A GeV O+C		390	22	76
60 A GeV O+Au		1326	139	608
200 A GeV O+Au				
central	$(0\% \leq E_{ZDC}/E_{beam} \leq 30\%)$	1730	229	1193
peripheral	$(40\% \leq E_{ZDC}/E_{beam} \leq 88\%)$	344	23	111

Table 1: Number of analyzed events N_{events}, reconstructed π^0, and reconstructed γ

hadron	rest mass (MeV/c^2)	decay channel	branching ratio (%)	Q-value (MeV/c^2)
π^0	134.9734	$\gamma\gamma$	98.798	134.9734
η	548.8	$\gamma\gamma$	38.90	548.8
		$\pi^+\pi^-\gamma$	4.91	269.7
ω	783	$\pi^0\gamma$	8.0	648
η'	958	$\rho^0\gamma$	30	188
		$\omega\gamma$	3	175
		$\gamma\gamma$	2.2	958
ϕ	1020	$\eta\gamma$	1.3	471.2
Σ^0	1192.5	$\Lambda\gamma$	100	76.9

Table 2: Compilation of hadrons with a rest mass less than 1500 MeV/c^2 and a branching ratio greater than 1% for radiative decays. [24]

	p_T (GeV/c)	value	reference
η/π^0	5	0.55	[28]
η'/π^0	5	1	[29]
ω/π^0	5	1	[29]
ϕ/π^0	2.8	0.075	[30, 31]

Table 3: Normalization points for Eq. 5 as used in Fig. 9

statistical error	$\pm 6\%$
geometrical π^0 acceptance	$\pm 3\%$
nonlinearity	$\pm 3\%$
photon reconstruction efficiency	$\pm(4-8)\%$
veto efficiency	$+0.1\%$
m_T scaling	$\pm 1\%$
η/π^0 induced error	
on the background calculation	$\pm 4\%$
quadratic sum	$\pm(9-12)\%$

Table 4: Systematic and statistical absolute errors of the γ/π^0 calculation

Figure captions

Fig. 1. Resolution of the invariant mass calculated from the energy and position resolution as measured in the calibration experiments. The calculation is shown as a function of the kinetic energy of the π^0 for symmetric (solid line) and asymmetric ($\alpha = 0.6$, see eq. 2, dashed line) π^0 decays. The experimental data are obtained for symmetric decays using a gaussian and polynomial function to fit the mass spectra

Fig. 2. Energy spectra of neutral and charged particles. In addition to the (kinetic) energy scale, an estimate of the corresponding transverse momentum scale is given

Fig. 3. Invariant mass spectra of $\gamma\gamma$ pairs for central 200 A·GeV ^{16}O+Au and minimum-bias 200 GeV p+Au reactions in different $p_T(\gamma,\gamma)$ bins :
a) 0.6 GeV/c $\leq p_T \leq$ 0.8 GeV/c; b) 1.0 GeV/c $\leq p_T \leq$ 1.2 GeV/c;
c) 1.4 GeV/c $\leq p_T \leq$ 1.6 GeV/c. Also shown are the polynomial background fits. Only photons with $E_\gamma \geq$ 500 MeV are considered

Fig. 4. Energy asymmetry α (solid circles) for minimum-bias 200 A·GeV ^{16}O+C events and five p_T regions. For comparison the Monte Carlo results are also shown (open squares)

Fig. 5. Photon reconstruction efficiencies for γ (κ_γ, dashed area, circles) and π^0 (κ_{π^0}, dotted area, triangles) as a function of the mean multiplicity of all hits μ_{all}. In addition, the efficiency to measure all photons as a resolved hit regardless whether a part of them are vetoed or not is shown as a solid area (squares). For the extraction of the data points see text. The arrows indicate the mean hit multiplicity μ_{all} from the following systems : 1. minimum-bias 200 GeV p+C , 2. minimum-bias 200 GeV p+Au , 3. minimum-bias 200 A·GeV ^{16}O+C , 4. peripheral 200 A·GeV ^{16}O+Au , 5. minimum-bias 60 A·GeV ^{16}O+Au , and 6. central 200 A·GeV ^{16}O+Au

Fig. 6. The π^0 p_T distribution from four times superimposed peripheral 200 A·GeV ^{16}O+Au events normalized to the π^0 p_T spectrum from peripheral 200 A·GeV ^{16}O+Au events. The invariant mass spectra for a) peripheral and b) four times superimposed events are shown as inserts for the p_T bin 0.8 GeV/c $\leq p_T \leq$ 1.2 GeV/c

Fig. 7. The p_T distribution of neutrons emitted into SAPHIR's solid angle as calculated by the event generator FRITIOF (solid line) and the simulated detector

response of these neutrons (shaded area). For comparison the photon p_T spectrum is also shown (dashed line)

Fig. 8. The transverse momentum of the hadrons η, η', ω, and Σ^0 is plotted versus the transverse momentum of the produced photons emitted into solid angle of SAPHIR

Fig. 9. Two different m_T-scalings as a function of p_T. η/π^0, η'/π^0, and ω/π^0 as created by eq. 4 for central (solid squares) and for peripheral (solid triangles) 200 A·GeV ^{16}O+Au reactions. For comparison eq. 5 is plotted as dashed lines using the values from Tab. 3 for normalization

Fig. 10. Invariant mass spectrum for minimum-bias 200 A·GeV ^{16}O+Au events in the transverse momentum interval 2.0 GeV/c $\leq p_T \leq$ 2.4 GeV/c. The fitted η peak is shown as an insert. An η/π^0 ratio of (61 $\pm$ 20) % is deduced from the spectrum

Fig. 11. Four different hadronic photon contributions normalized to the π^0 yield as a function of p_T calculated by a Monte Carlo simulation

Fig. 12. Estimate for fake direct photons arising from the decay $K_S^0 \rightarrow \pi^0\pi^0$. For the explanation of the three plots see text

Fig. 13. Transverse momentum distributions of π^0's and photons from the event generator FRITIOF 1.6 (solid squares), the experimental data (solid circles), and the Monte Carlo simulation (histograms) for a) peripheral and b) central 200 A·GeV ^{16}O+Au events. The inserts show the Monte Carlo simulations normalized to the experimental data

Fig. 14. Ratio of inclusive photon cross section to π^0 cross section as a function of transverse momentum for 200 GeV p+C , 200 GeV p+Au , 200 A·GeV ^{16}O+C , and 60 A·GeV ^{16}O+Au events under minimum-bias trigger conditions. The squares indicate the data, and the shaded histograms are the Monte Carlo results representing hadronic decays

Fig. 15. Ratio of inclusive photon cross section to π^0 cross section as a function of transverse momentum for central and peripheral 200 A·GeV ^{16}O+Au reactions. The squares indicate the data, and the shaded histograms are the Monte Carlo results representing hadronic decays. The data from peripheral events show a slight

enhancement around $p_T = 1.6$ GeV/c. We believe this to be an artifact of the detailed efficiency for events selected by the high-p_T trigger

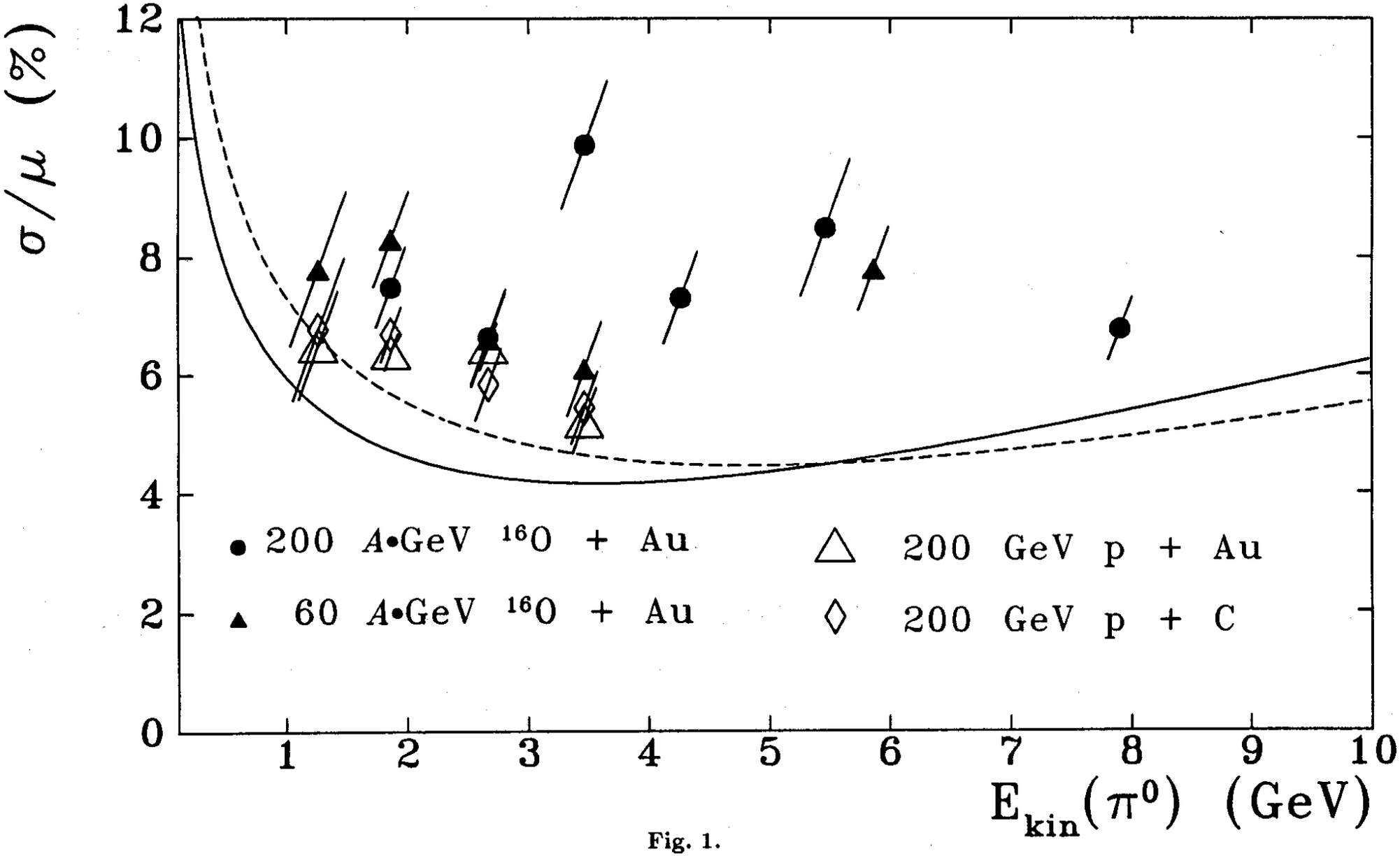
σ/μ (%)
12
10
8
6
4
2
0
1
2
3
4
5
6
7
8
9
10
E_kin(π⁰) (GeV)
200 A•GeV ¹⁶O + Au
60 A•GeV ¹⁶O + Au
200 GeV p + Au
200 GeV p + C

Fig. 1.

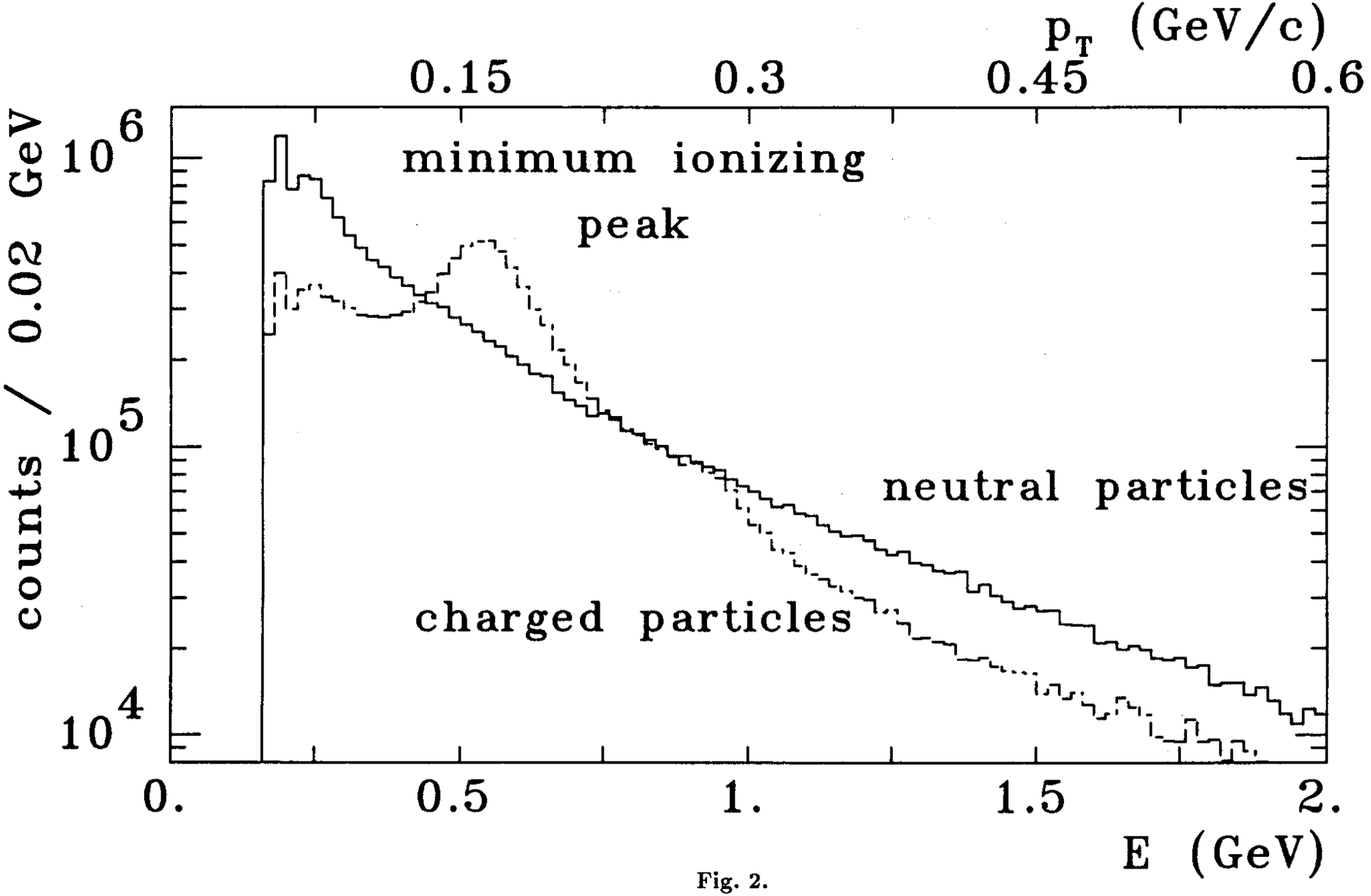
p_T (GeV/c)
0.15
0.3
0.45
0.6
minimum ionizing
peak
neutral particles
charged particles
counts / 0.02 GeV
10^6
10^5
10^4
0.
0.5
1.
1.5
2.
E (GeV)

Fig. 2.

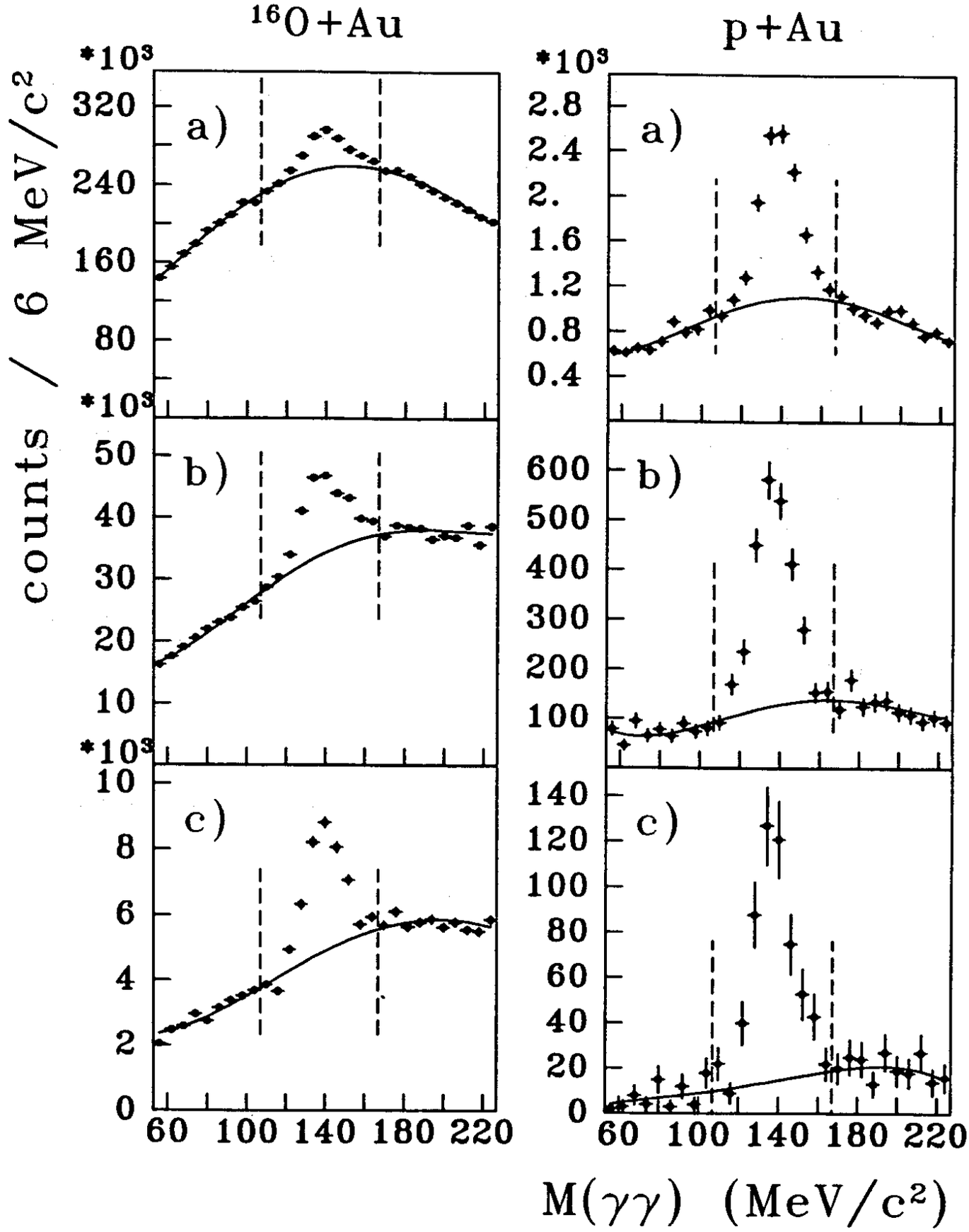
^{16}O+Au
p+Au
counts / 6 MeV/c^2
*10^3
320
240
160
80
a)
50
40
30
20
10
b)
10
8
6
4
2
0
c)
2.8
2.4
2.
1.6
1.2
0.8
0.4
600
500
400
300
200
100
140
120
100
80
60
40
20
60 100 140 180 220
M($\gamma\gamma$) (MeV/c^2)

Fig. 3.

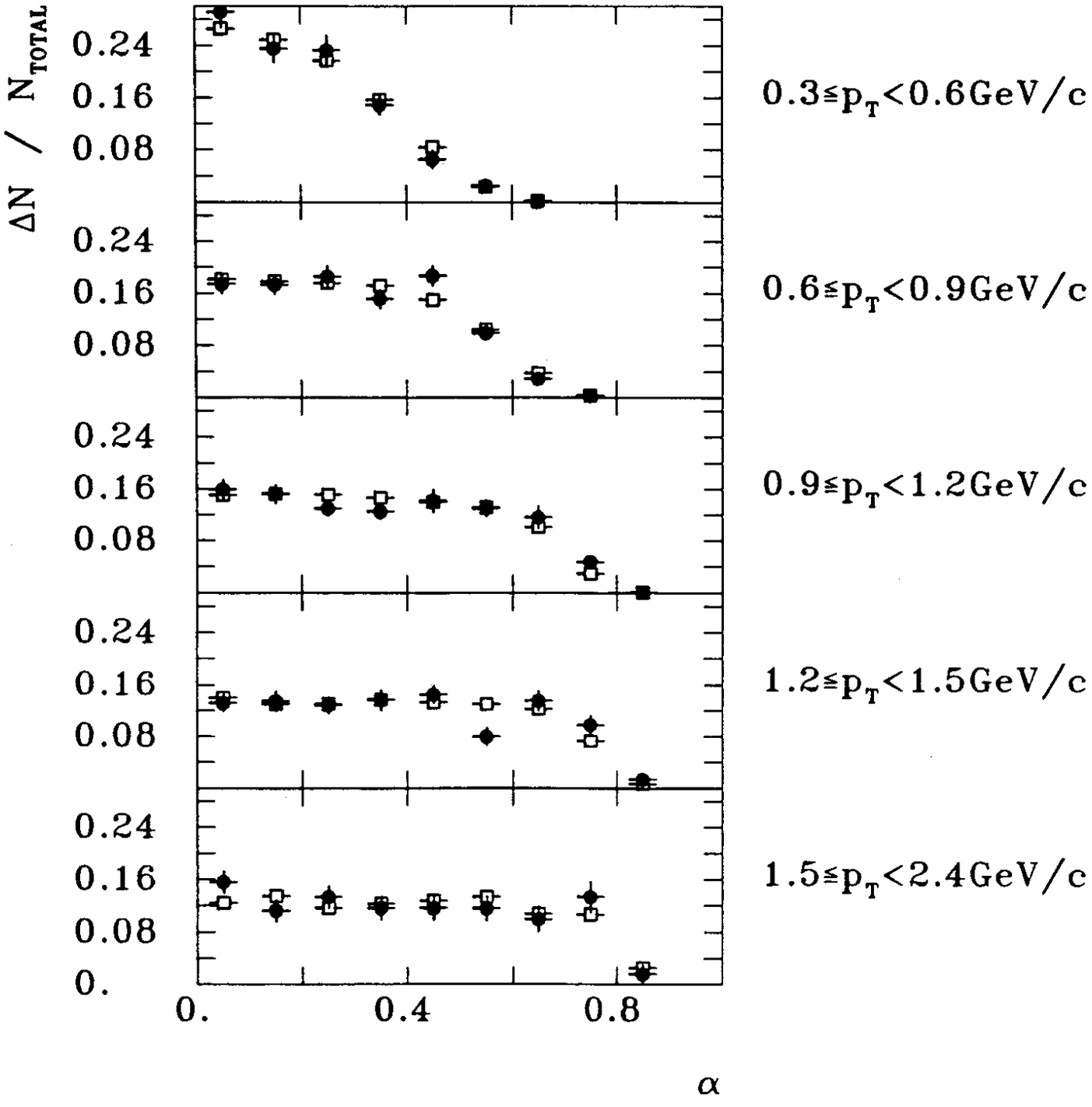
ΔN / N_TOTAL
0.24
0.16
0.08
0.24
0.16
0.08
0.24
0.16
0.08
0.24
0.16
0.08
0.24
0.16
0.08
0.
0.
0.4
0.8
α
0.3≤p_T<0.6GeV/c
0.6≤p_T<0.9GeV/c
0.9≤p_T<1.2GeV/c
1.2≤p_T<1.5GeV/c
1.5≤p_T<2.4GeV/c

Fig. 4.

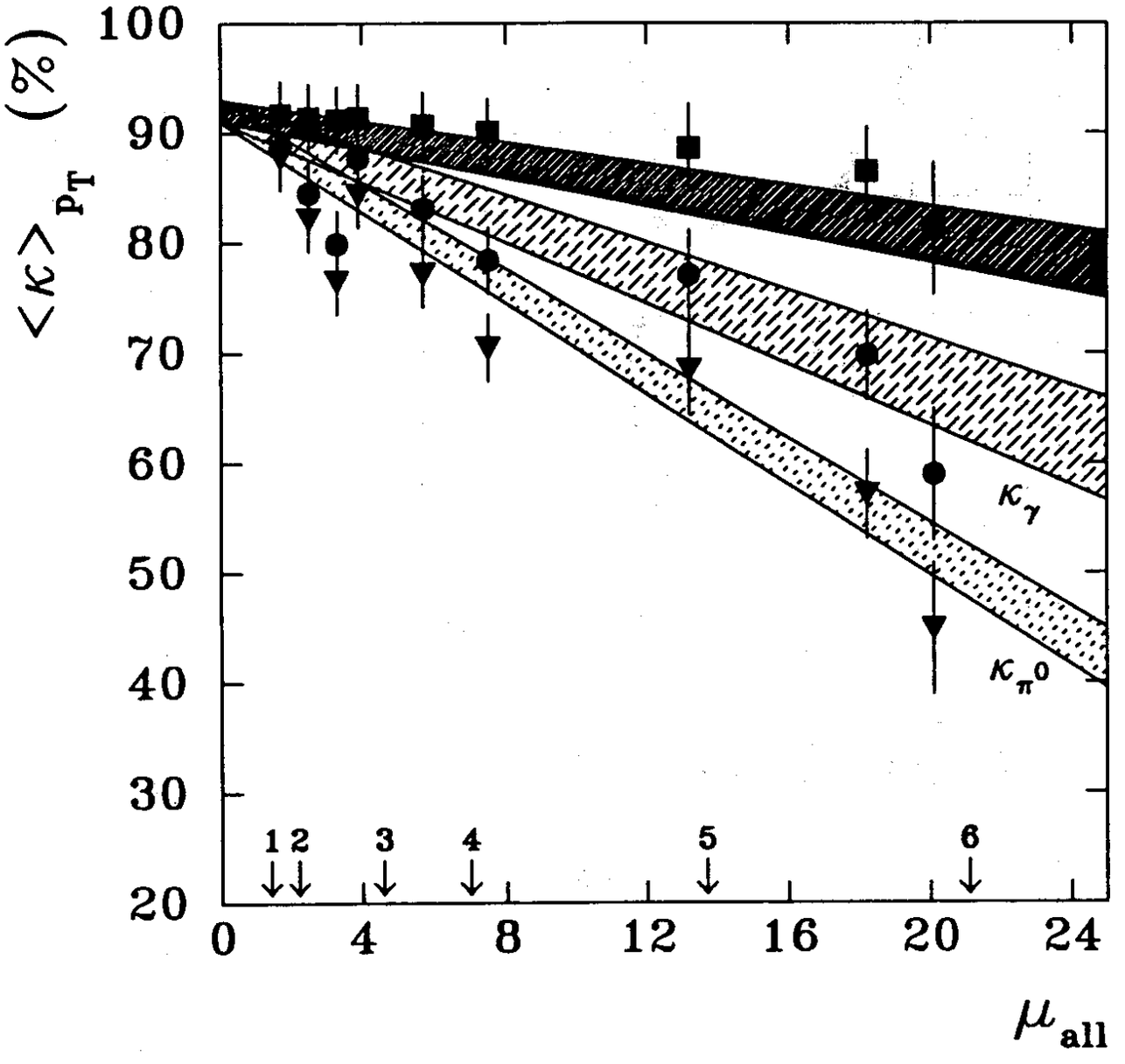
100
90
80
70
60
50
40
30
20
$\langle \kappa \rangle_{p_T}$ (%)
0
4
8
12
16
20
24
μ_{all}
1 2
3
4
5
6
κ_γ
κ_{π^0}

Fig. 5.

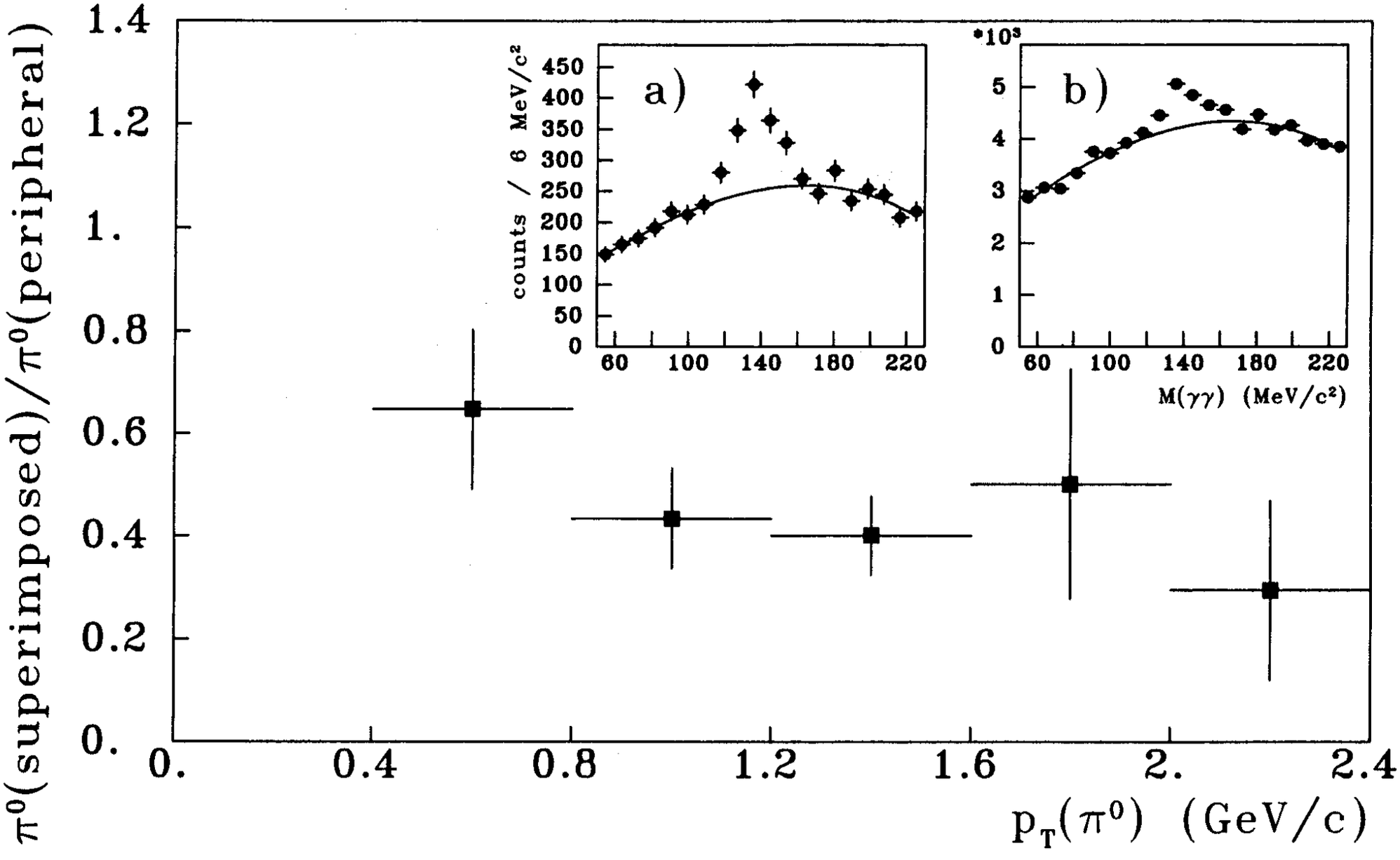
π^0(superimposed)/π^0(peripheral)
1.4
1.2
1.
0.8
0.6
0.4
0.2
0.
0.
0.4
0.8
1.2
1.6
2.
2.4
$p_T(\pi^0)$ (GeV/c)
a)
counts / 6 MeV/c²
450
400
350
300
250
200
150
100
50
0
60
100
140
180
220
b)
*10³
5
4
3
2
1
0
60
100
140
180
220
M(γγ) (MeV/c²)

Fig. 6.

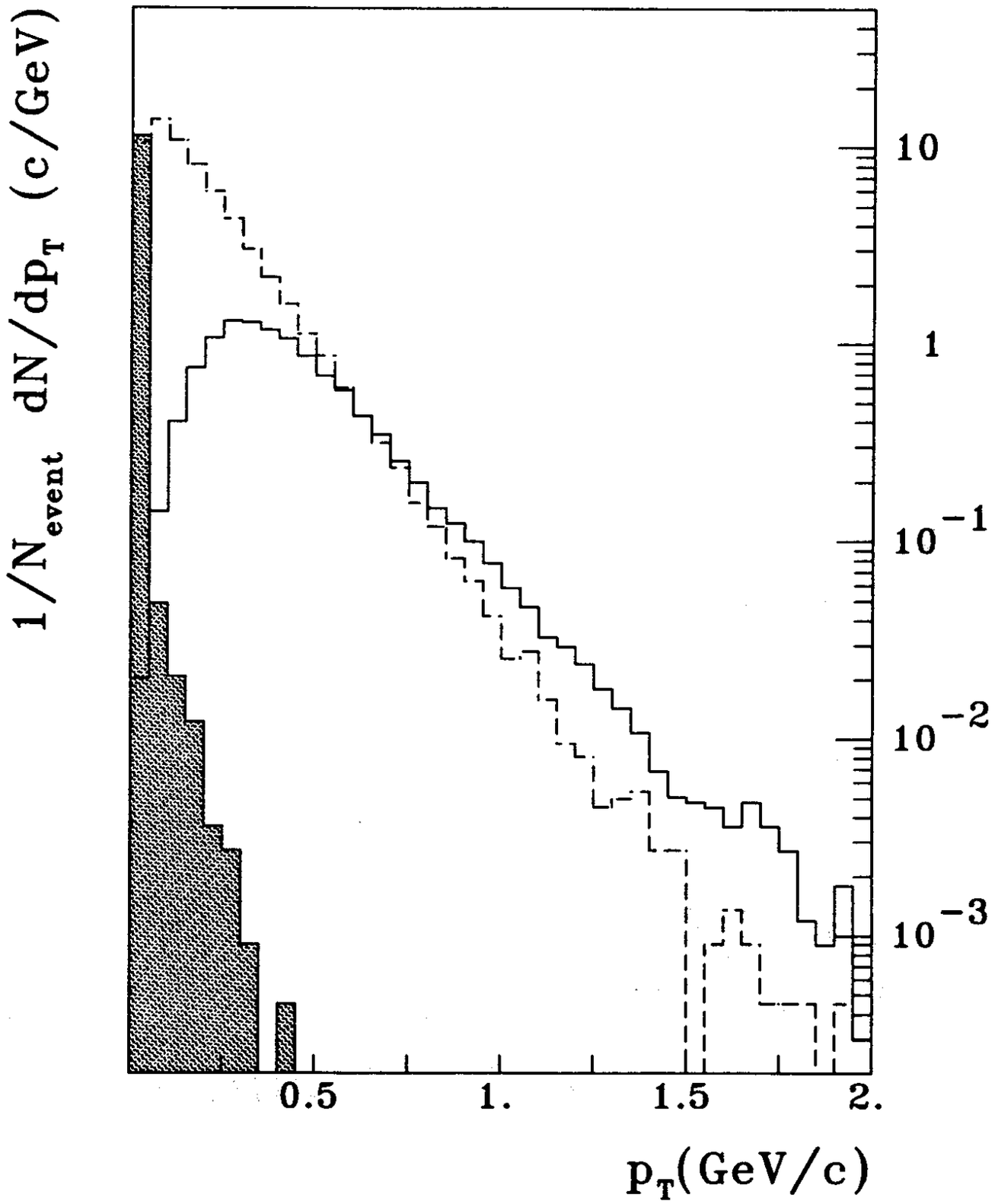

Fig. 7.

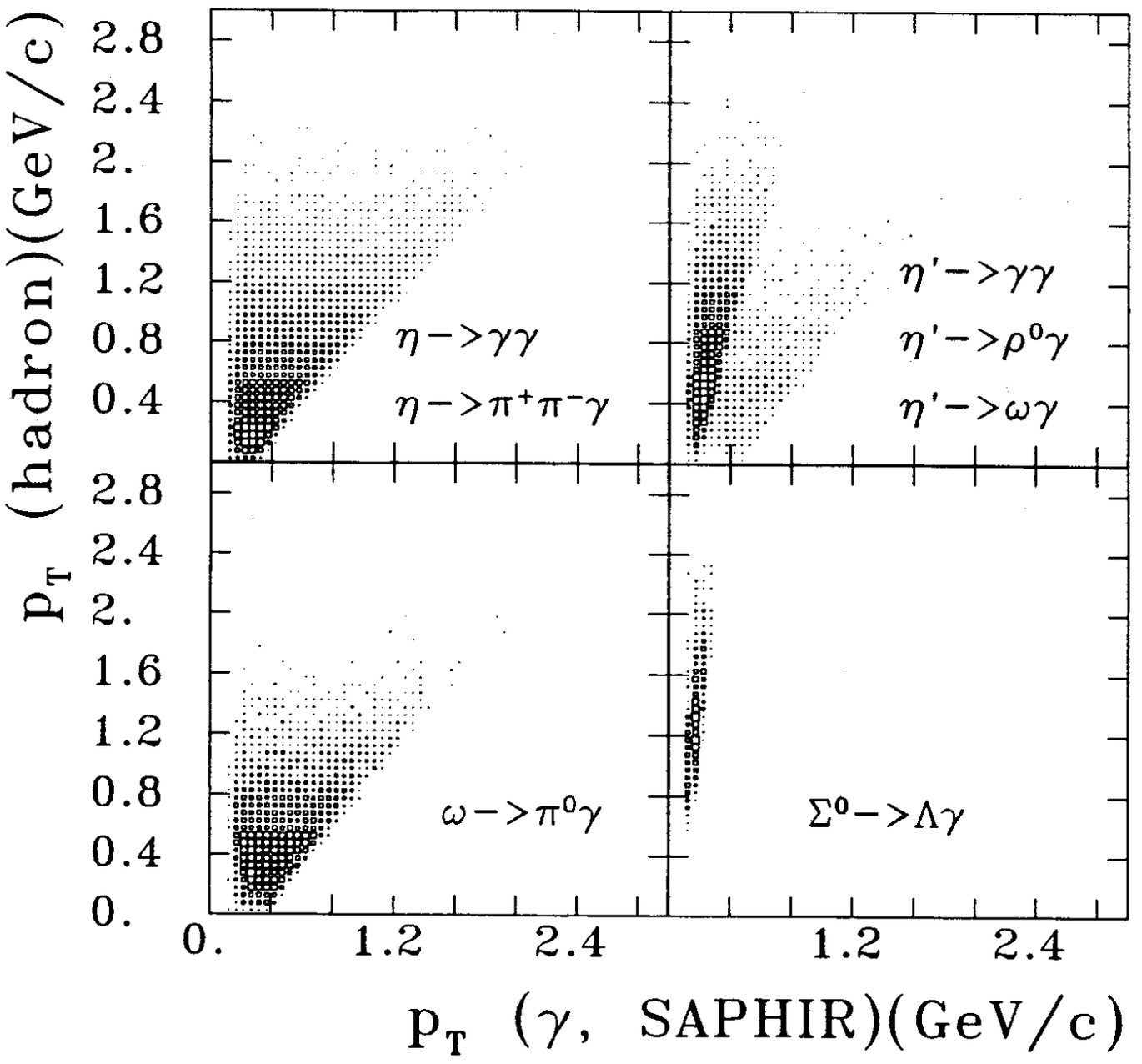
p_T (hadron)(GeV/c)
2.8
2.4
2.
1.6
1.2
0.8
0.4
0.
$\eta -> \gamma\gamma$
$\eta -> \pi^+\pi^-\gamma$
$\eta' -> \gamma\gamma$
$\eta' -> \rho^0\gamma$
$\eta' -> \omega\gamma$
$\omega -> \pi^0\gamma$
$\Sigma^0 -> \Lambda\gamma$
0.
1.2
2.4
p_T (γ, SAPHIR)(GeV/c)

Fig. 8.

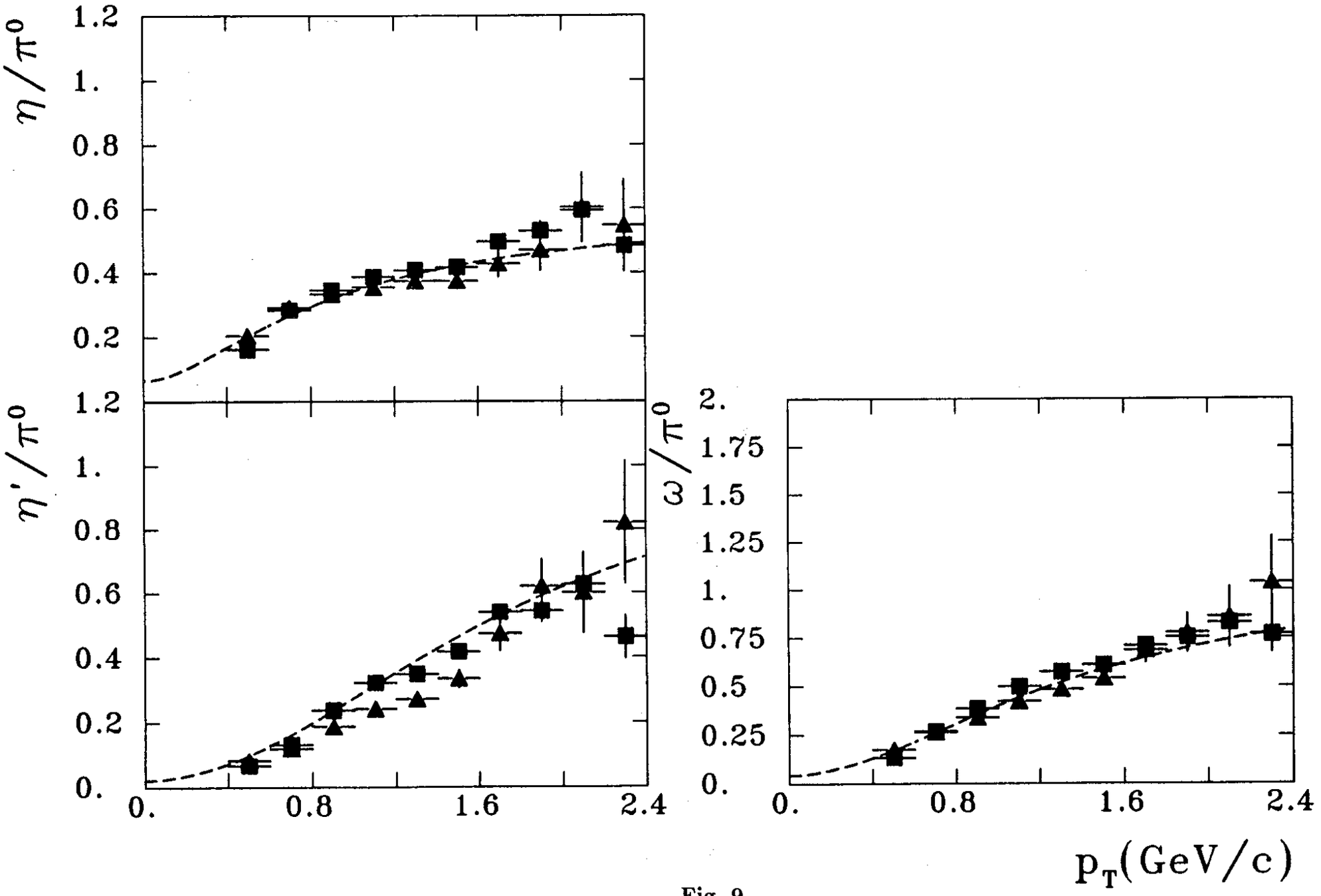
η/π^0
η'/π^0
ω/π^0
1.2
1.
0.8
0.6
0.4
0.2
0.
2.
1.75
1.5
1.25
0.75
0.5
0.25
0.8
1.6
2.4
p_T(GeV/c)

Fig. 9.

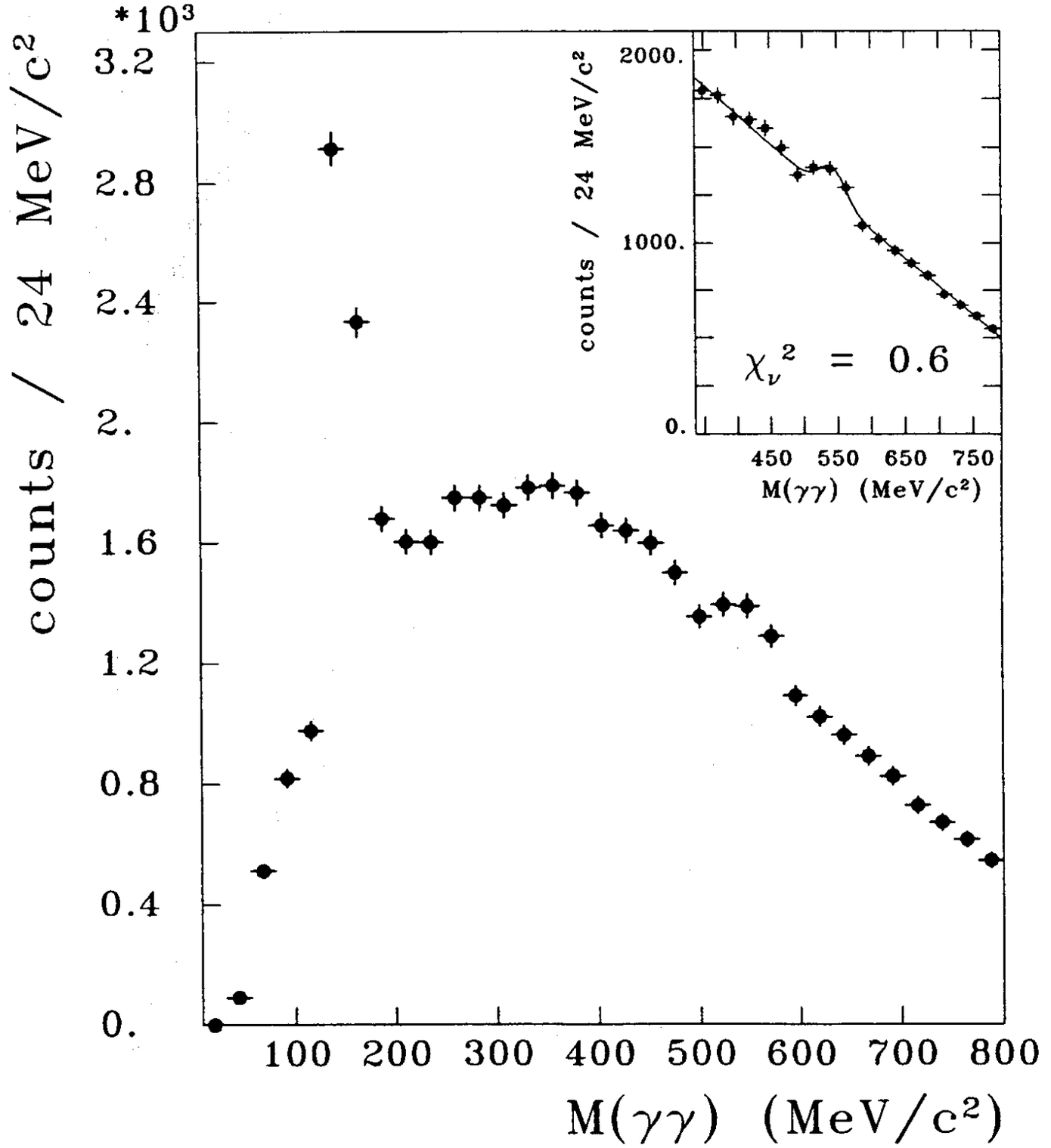
*10³
3.2
2.8
2.4
2.
1.6
1.2
0.8
0.4
0.
counts / 24 MeV/c²
100 200 300 400 500 600 700 800
M(γγ) (MeV/c²)
2000.
1000.
0.
counts / 24 MeV/c²
χν² = 0.6
450 550 650 750
M(γγ) (MeV/c²)

Fig. 10.

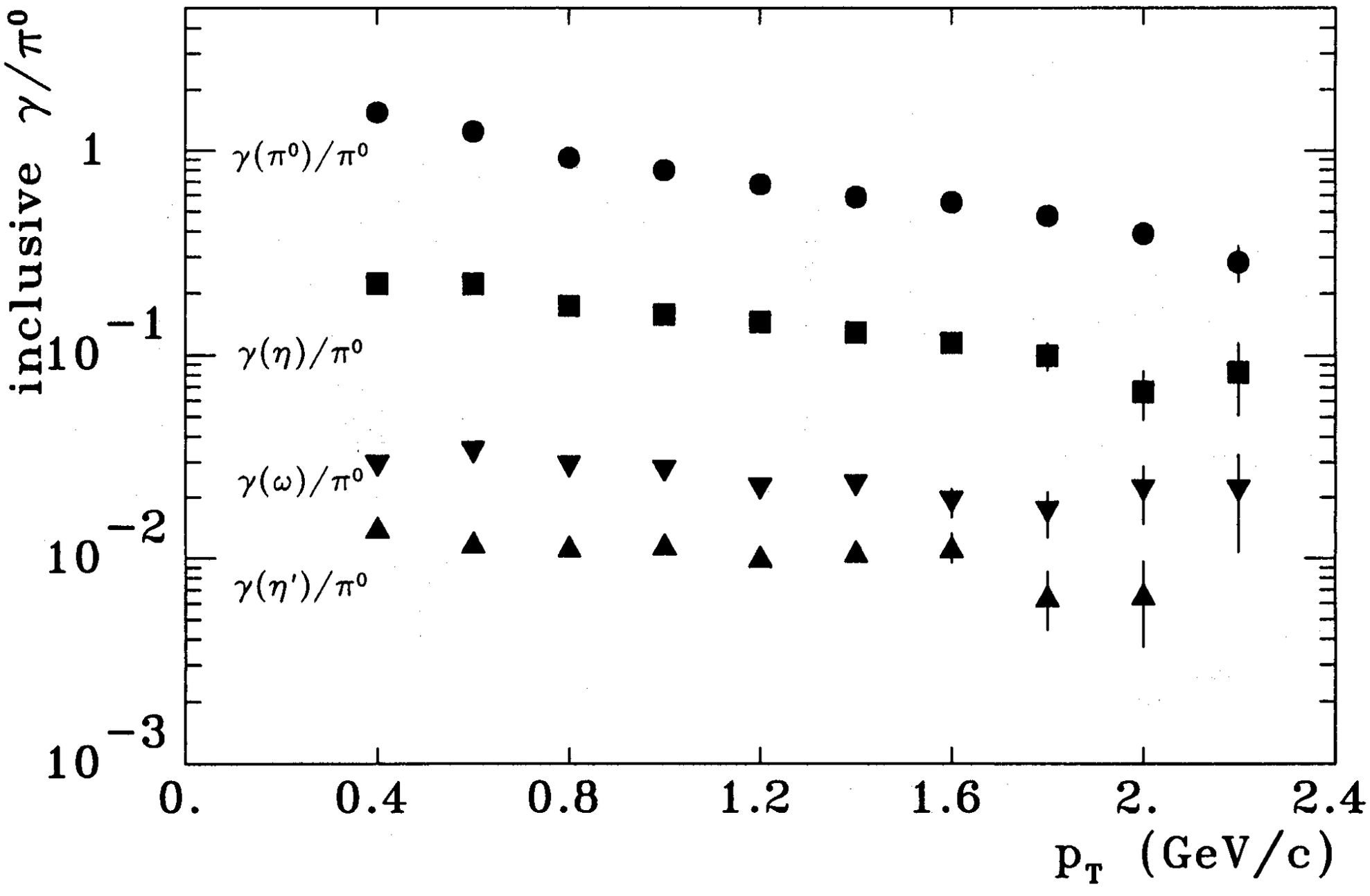
inclusive γ/π^0
1
10^{-1}
10^{-2}
10^{-3}
$\gamma(\pi^0)/\pi^0$
$\gamma(\eta)/\pi^0$
$\gamma(\omega)/\pi^0$
$\gamma(\eta')/\pi^0$
0.
0.4
0.8
1.2
1.6
2.
2.4
p_T (GeV/c)

Fig. 11.

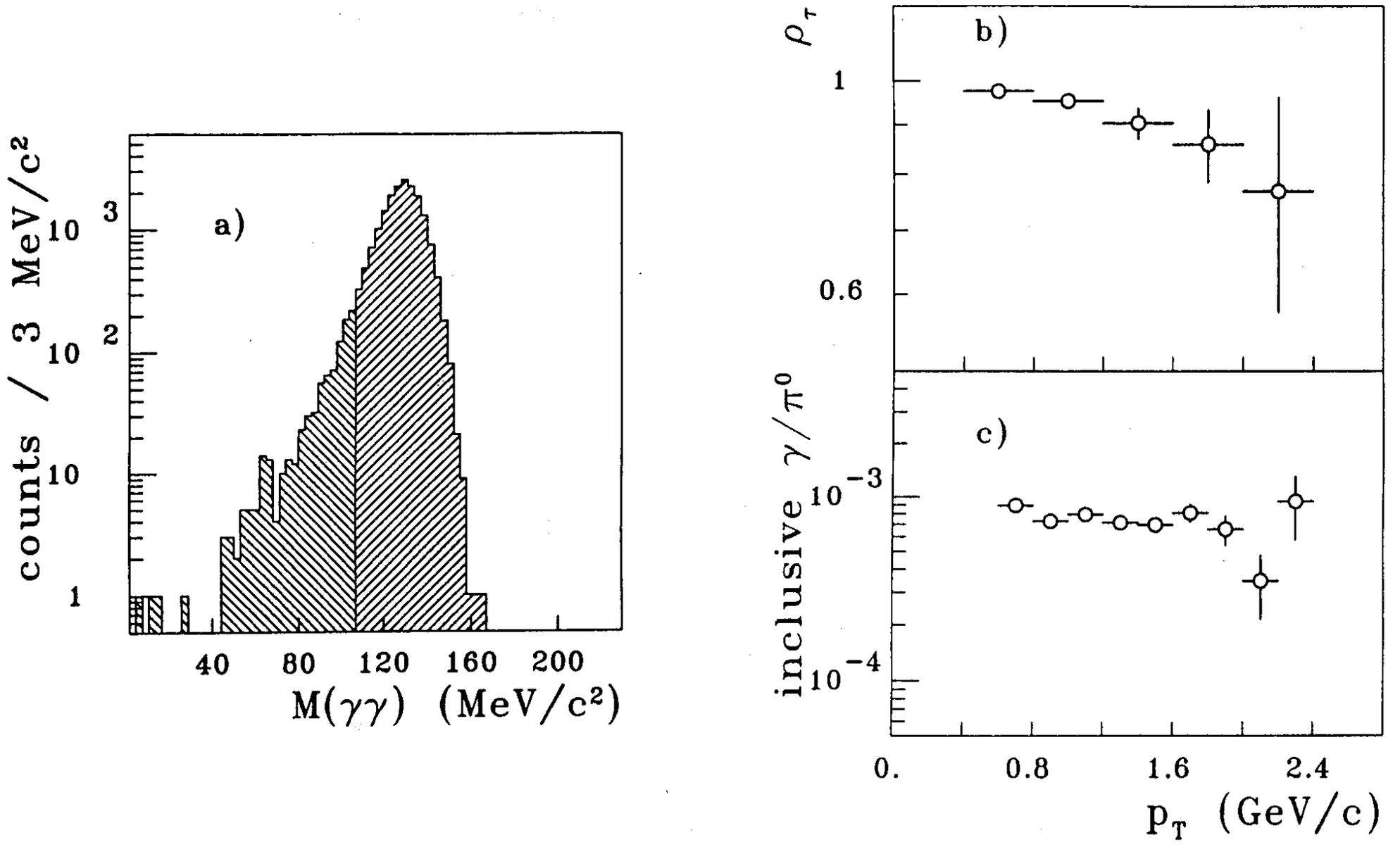
a)
counts / 3 MeV/c²
10³
10²
10
1
40
80
120
160
200
M(γγ) (MeV/c²)
b)
ρ_T
1
0.6
c)
inclusive γ/π⁰
10⁻³
10⁻⁴
0.
0.8
1.6
2.4
p_T (GeV/c)

Fig. 12.

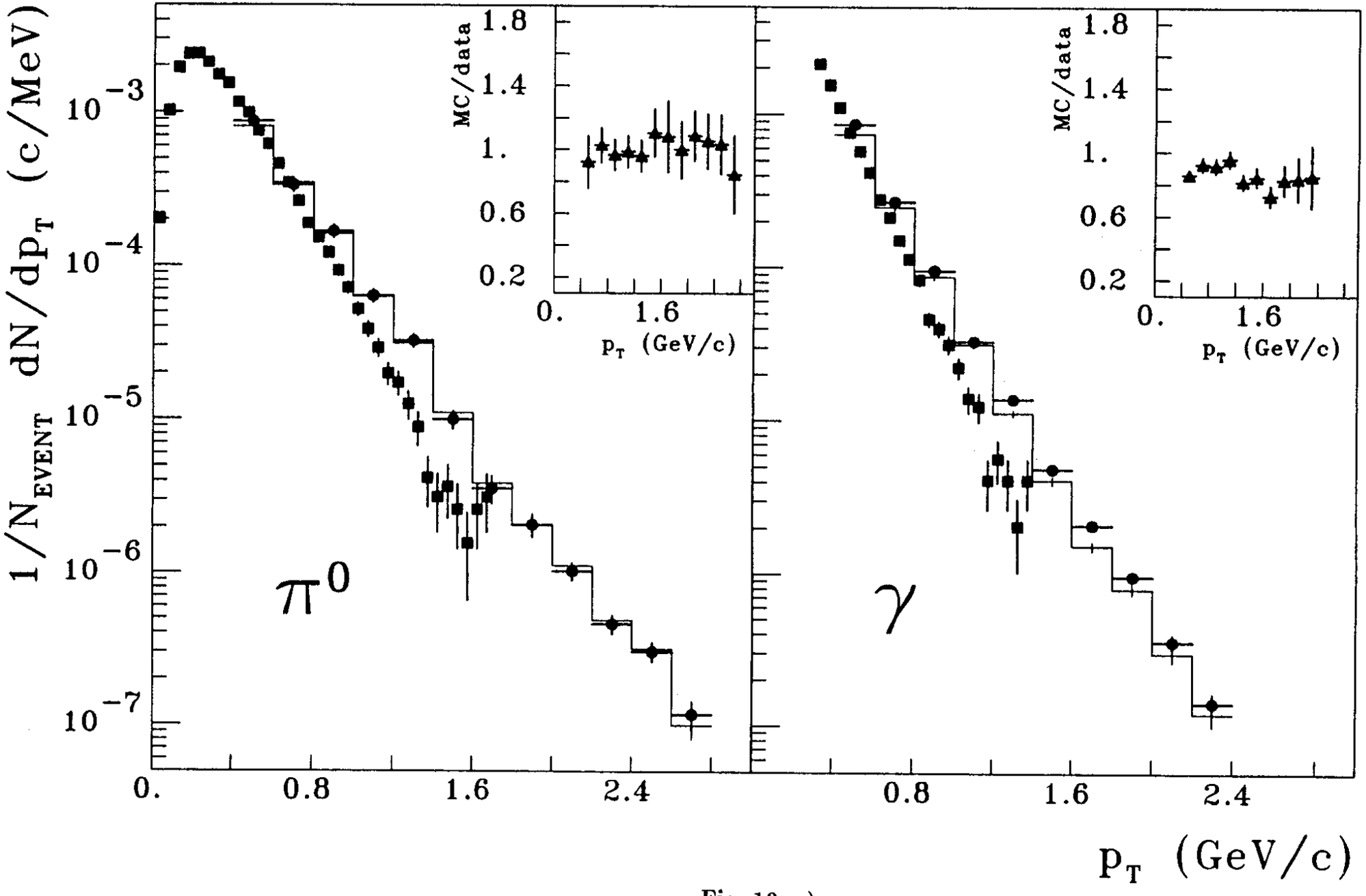
$1/N_{EVENT}\ dN/dp_T\ (c/MeV)$
10^{-3}
10^{-4}
10^{-5}
10^{-6}
10^{-7}
π^0
γ
MC/data
1.8
1.4
1.
0.6
0.2
0.
1.6
p_T (GeV/c)
0.
0.8
1.6
2.4
p_T (GeV/c)

Fig. 13. a)

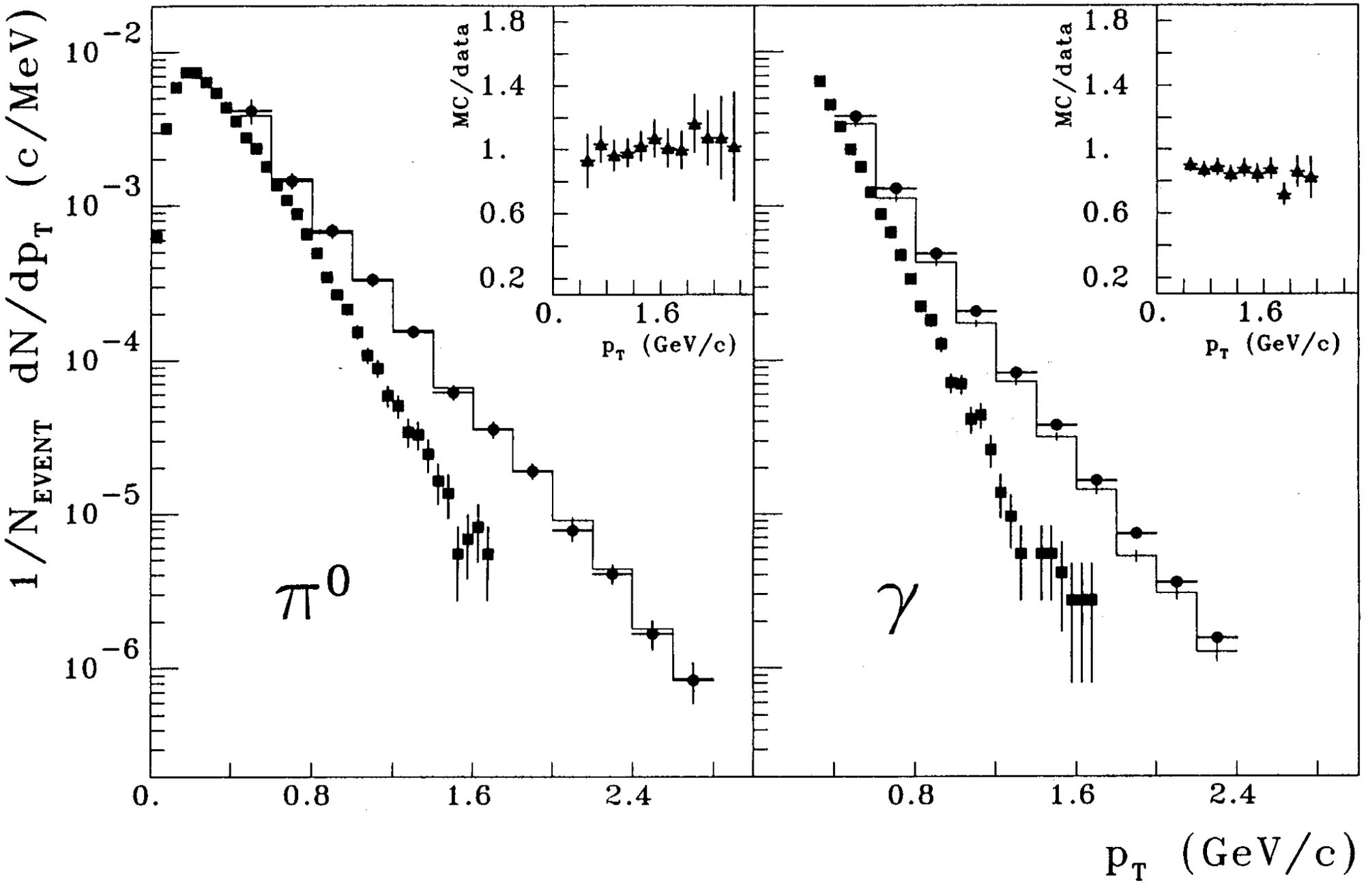
$1/N_{EVENT}\ dN/dp_T\ (c/MeV)$
10^{-2}
10^{-3}
10^{-4}
10^{-5}
10^{-6}
π^0
γ
MC/data
1.8
1.4
1.
0.6
0.2
0.
1.6
p_T (GeV/c)
0.
0.8
1.6
2.4
p_T (GeV/c)

Fig. 13. b)

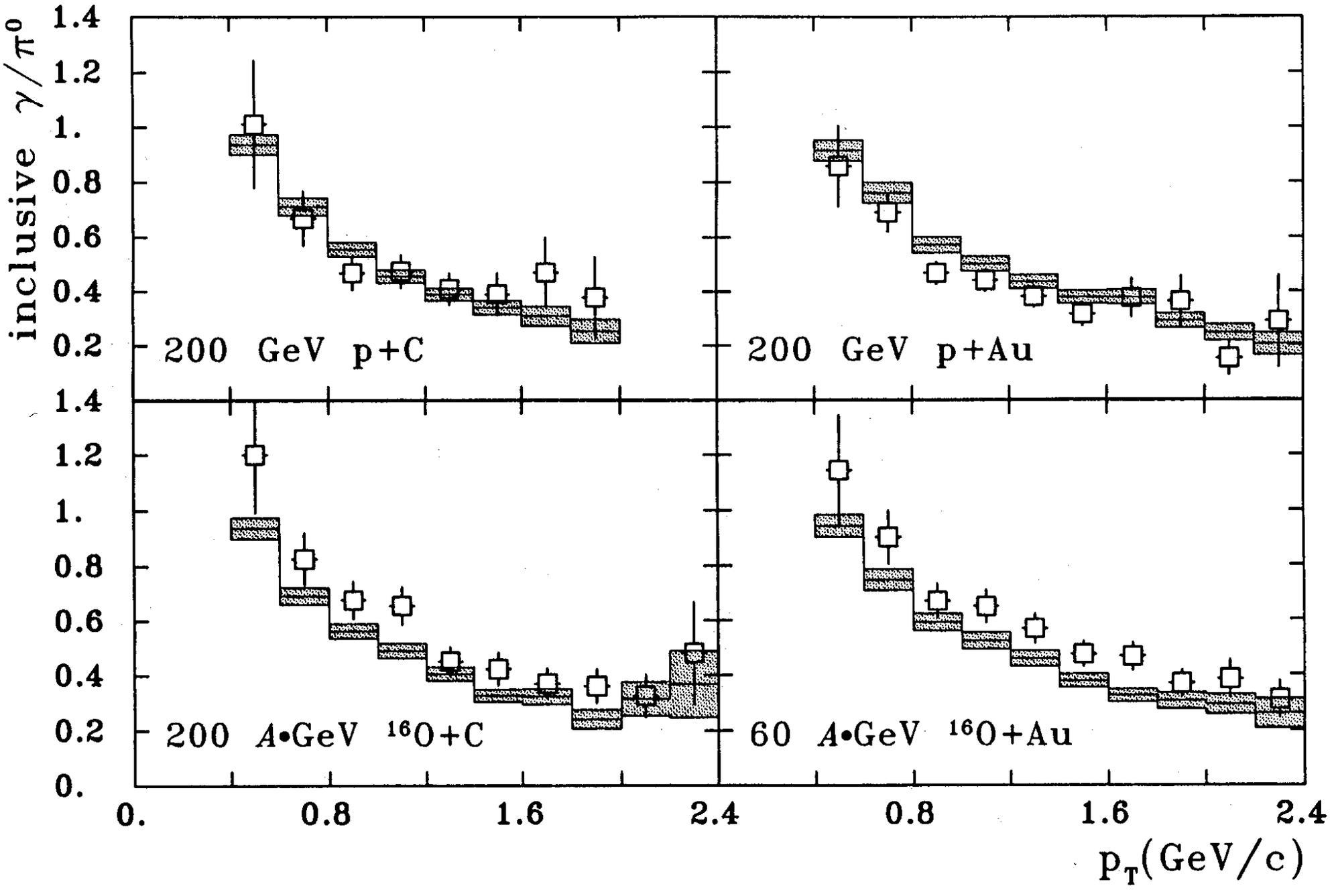
inclusive γ/π^0
200 GeV p+C
200 GeV p+Au
200 A•GeV ^{16}O+C
60 A•GeV ^{16}O+Au
p_T(GeV/c)
0.
0.2
0.4
0.6
0.8
1.
1.2
1.4
1.6
2.4

Fig. 14.

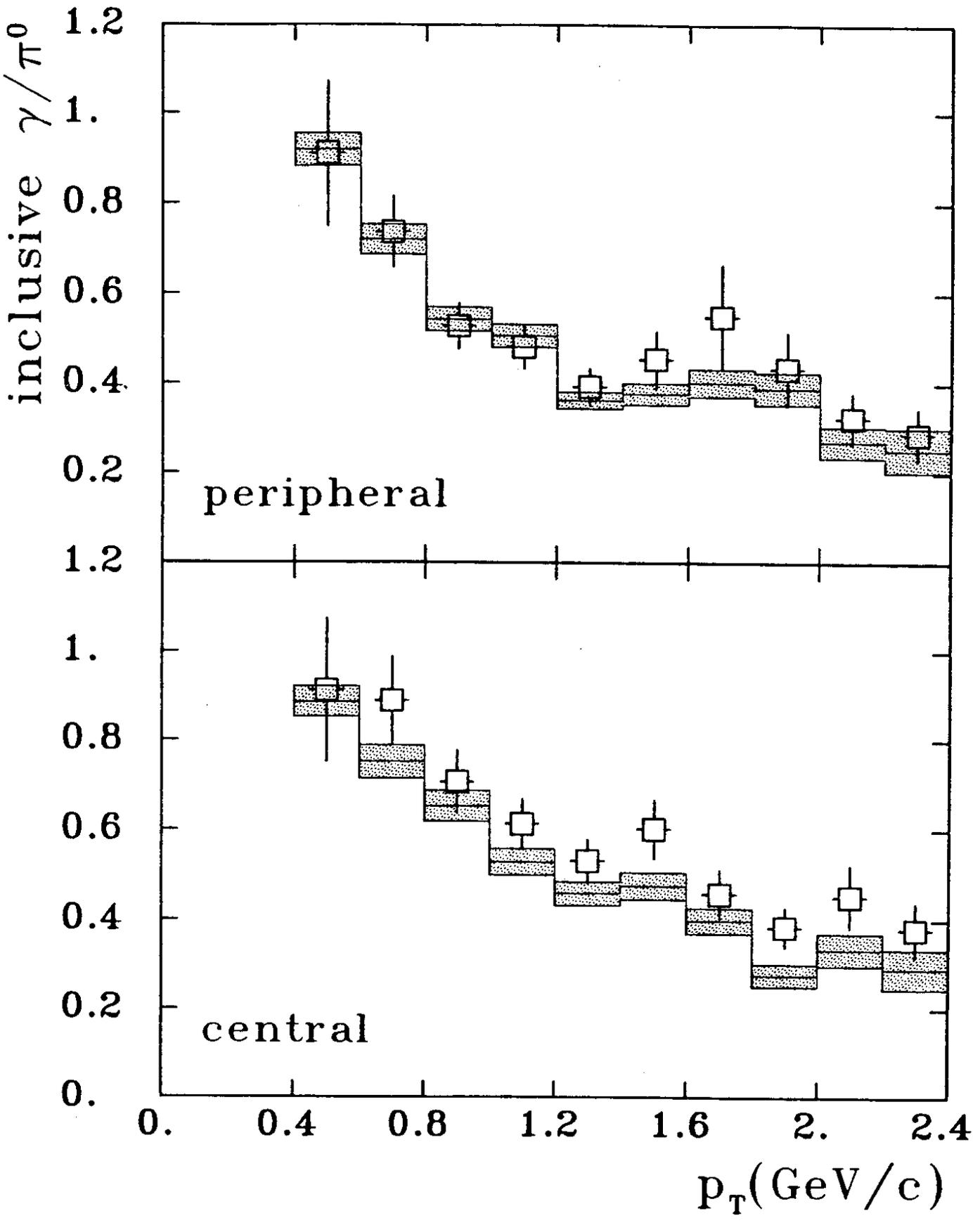

Fig. 15.

Imprimé au CERN. Prix : 1.15 Fr.